Electronic Supplementary Material (ESI) for ChemComm.

Supporting Information

The Enhanced Electrochemical CO_2 Reduction Performance of Cobalt Phthalocyanine with Precise Electronic States Regulation

Tong Yao[a], Lu-Hua Zhang[a,*], Jiayu Zhan[a], Zhixiang Zhou[a], Yang You[a], Zisheng Zhang[a], Fengshou Yu[a,*]

[a] National-Local Joint Engineering Laboratory for Energy Conservation in Chemical Process Integration and Resources utilization, School of Chemical Engineering and Technology, Hebei University of Technology, Tianjin 300130, P. R. China

***Corresponding Authors:**

E-mail address: luhuazhang@hebut.edu.cn (L.-H. Zhang); yfsh@hebut.edu.cn (F. Yu)

1. Experimental Procedures

1.1 DFT calculations

Structure relaxation, vibrational frequency analysis, and single-point energies were calculated using DFT as implemented in the DMOL^3 program. The Perdew-Burke-Ernzerhof (PBE) functional within the formulation of generalized gradient approximation (GGA) was used to handle the exchange and correlations, and the Grimme parameters for van der Waals dispersion correction was also added to all calculations. The electrons of metal atom were described by semi-core pseudopotentials (DSPPs) and a double numerical plus polarization (DNP) basis set. In the present work, the light element including C, O, N, and H atoms were treated with all-electron basis set, while the core metal (Co) electrons were treated with DSPPs and the metal valence electrons were evaluated with DNP basis set. A Gaussian smearing finite temperature broadening method (=0.005 Ha) is used during structural optimizations. To ensure high-quality results, the real space atomic cutoff radius is chosen as 4.5 Å for Co respectively. Kohn-Sham self-consistent field calculations are performed with convergence tolerance of 1×10^{-6} Ha on the total energy. The free energy diagrams of ECRR and HER were estimated using the Nørskov equation.[1]

1.2 Computational Hydrogen Electrode (CHE) Model

The core idea of the CHE model is that the Gibbs free energy of the proton-electron pairs ($H^+ + e^-$) related in the PECT progress can be referenced by the free energy of gaseous H_2, whereas the fact that the proton-electron pairs is in equilibrium with gaseous H_2 at 0 V versus standard hydrogen electrode (U = 0, pH = 0, and pressure = 1 bar, and temperature = 298.15 K). Accordingly, the chemical potential of H_2 (g) is equal to that of $H^+ + e^-$;

$$\mu\,(H_2(g)) = 2\,\mu\,(H^+ + e^-)$$

The effect of the applied bias U can be accounted by the following formula:

$$\mu\,(H_2(g)) = 2\,\mu\,(H^+ + e^- + eU)$$

Theoretically, the reaction pathway in electrochemical reduction of CO_2 to CO following the progresses:

$$CO_2\ (g) + * + e^- \longrightarrow *CO_2^-\ (1)$$

$$*CO_2^- + H^+ \longrightarrow *COOH\ (2)$$

$$*COOH + e^- + H^+ \longrightarrow *CO + H_2O\ (3)$$

$$*CO \longrightarrow CO\ (g) + *\ (4),$$

in which the asterisk refers to the clean catalysis, and the asterisk-marked one refers to the species that adsorbed on the activity center.

The free energy change ΔG_1 under the zero overpotential for the first proton-coupled electron-transfer step can be calculated with the equation

$\Delta G_1 = \Delta E + \Delta ZPE + \Delta_{0\rightarrow 298K}H - T\Delta S$

$= \Delta E_{\ total} + \Delta G_{\ corr}\,(298K)$

$= [E_{\ total}\,(COOH^*) - E_{\ total}\,(CO_2 + 1/2\ H_2 + *)] + [G_{\ corr}\,(298K)\,(COOH^*) - G_{\ corr}\,(298K)\,(CO_2 + 1/2\ H_2 + *)]$

Where the E_{total} and $G_{corr}\,(298K)$ is the calculated total electron energy and free energy correction that includes the zero-point energies (ZPE).

Similarly, we can get the equation for ΔG_2 of the second proton-coupled electron-transfer step

$\Delta G_2 = [E_{total}\,(CO^* + H_2O) - E_{total}\,(COOH^*) + 1/2H_2)] + [G_{corr}\,(298K)\,(CO^* + H_2O) - G_{corr}\,(298K)\,(COOH^*) + 1/2H_2)]$

the finally step for CO desorption step can be calculated as

$\Delta G_3 = [E_{total}\,(CO + *) - E_{total}\,(CO^*)] + [G_{corr}\,(298K)\,(CO + *) - G_{corr}\,(298K)\,(CO^*)]$

1.3 Chemicals and Materials

1.3.1 Synthesis of R-GQD:

In a typical procedure for the synthesis of NH_2-GQD, pyrene (2 g) was stirred in HNO_3 (160 mL) at 80 °C for 12 h. After cooling to room temperature, the mixture was diluted

with excess deionized water and passed through a 0.22 μm pore size filter to remove acid. The resulted yellow product was dispersed in an aqueous solution containing ammonia (0.6 L, 0.2 M) and sonicated for 2 h. The suspension was then transferred to a Teflon-lined autoclave (1 L) and heated at 200 °C for 10 h. After cooling to room temperature, the product containing water-soluble NH_2-GQD was passed through a 0.22 μm pore size filter membrane to remove insoluble carbon products and further dialyzed in a dialysis bag for 2 days to remove undissolved small molecules. The synthetic procedure of OH-GQD was similar to that of the NH_2-GQD except for the addition of different alkaline species in the media: 0.2 M NaOH.

1.3.2 Synthesis of NH_2-GNS:

According to the study of James M. Tour et al., GNS was successfully prepared[2]. Nitration modification of the GNS sample was performed according to a previously reported method. 30 mL of fuming nitric acid was slowly dripped into a suspension of 1 g of GNS and 40 mL of acetic anhydride in a 1000 mL three-necked flask at 0 ℃. After stirring at this temperature for 5 h and subsequently stirring for 19 h at 20 ℃, the solid sample was filtrated and washed until the filtrate was neutral. When dry for 12 h, add the solid powder to 10 mL of strong aqua ammonia and 20 mL of pure water. After adding 0.75 g of sodium borohydride, the suspension was kept at 20 ℃ for 24 h under stirring. The solid was filtrated, washed until the filtrate was neutral, and then dried at 105 ℃ for 12 h[3]. The obtained sample was labeled GNS–NH_2. In addition, amino-graphene (NH_2-G, amine ratio 4 wt%) were purchased from Aladdin Industrial Inc.

1.3.3 Synthesis of CoPc/R-GQD, CoPc/NH_2-GNS and CoPc/NH_2-G:

10 mg of the R-GQD was dispersed in 30 mL of DMF with sonication (500 W, 40 kHz). Then, CoPc (10 mg) dissolved in DMF was added to the R-GQD suspension. The mixture was sonicated for 30 min to obtain a fully mixed suspension, which was further stirred at room temperature for 20 h. Subsequently, the mixture was centrifuged and the precipitate was washed with DMF and ethanol. Finally, the precipitate was vacuum dried to yield the final product. The synthesis process of CoPc/NH_2-GNS and

CoPc/NH_2-G is similar to that of CoPc/R-GQD, except that the carrier was changed into NH_2-GNS and NH_2-G.

1.4 Electrochemical Measurements:

All electrochemical measurements in this work were performed in a conventional three-electrode cell using CHI760E electrochemical workstation. 4.0 mg of catalyst was dissolved in mixture solution containing 475 μL of ethanol, 475 μL of ultrapure water, and 50 μL of Nafion solution (5 wt%), and sonicated for 30 min. Then, electrocatalyst ink was dropped on the carbon paper to achieve a loading of 0.6 mg cm^{-2}. The compartment of the H-type electrolytic cell used in the ECRR experiment was separated by an ion exchange membrane, with Ag/AgCl as the reference electrode, platinum wire as the counter electrode, and the 1 cm^2 carbon paper with catalyst as the working electrode. Electrode potentials were converted to the RHE by the followed equation: E (versus RHE) = E (versus Ag/AgCl) + 0.224 V + 0.0596 × pH.

2. Supplementary figures

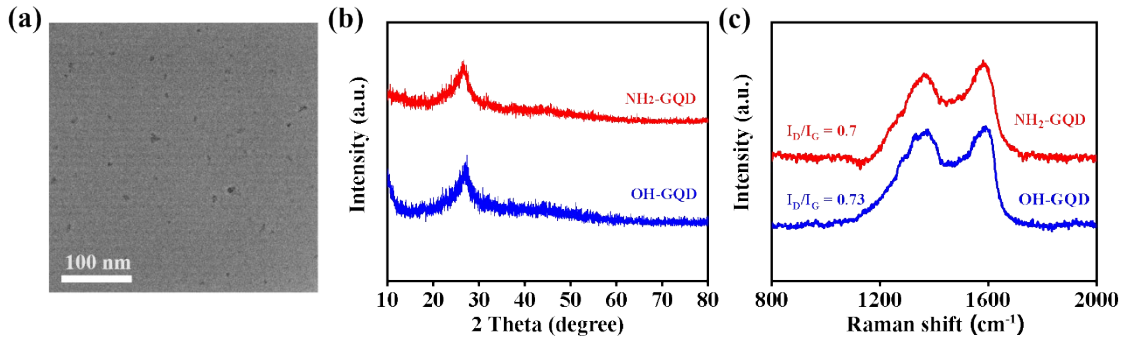

Figure S1. (a) TEM image of OH-GQD; (b) XRD patterns of NH_2-GQD and OH-GQD; (c) Raman spectra of NH_2-GQD and OH-GQD.

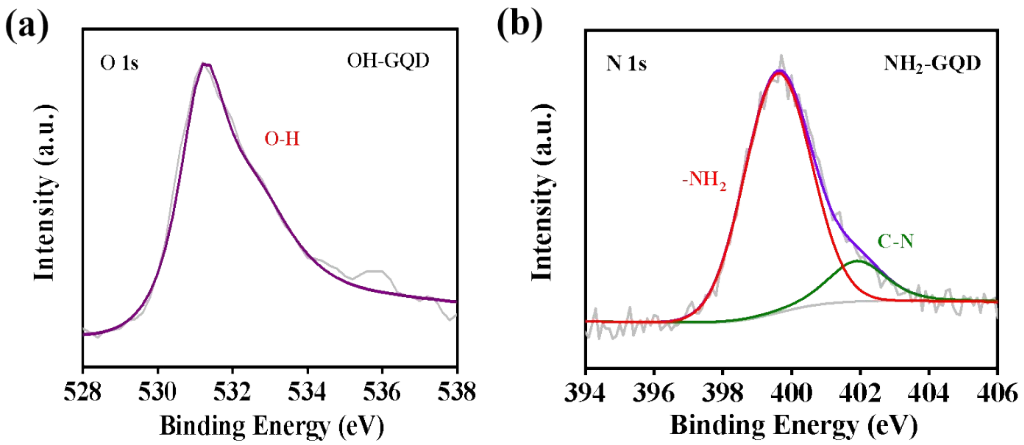

Figure S2. (a) O 1s XPS spectrum of OH-GQD; (b) N 1s XPS spectra of NH_2-GQD.

The high-resolution O 1s spectrum (Figure S2a) reveals the presence of O-H at 531.4 eV. The XPS analysis demonstrates that 1,3,6-trinitropyrene is fused into OH-GQD by total removal of the NO_2 group under the strongly alkaline hydrothermal conditions. The high-resolution N 1s spectrum reveals the signals of -NH_2 at 399.6 eV and N-C at 401.9 eV and the GQD-NH_2 contains a total of N atomic content of 9.8 at.% (Figure S2b). All these results indicates that the successful synthesis of NH_2- and OH-functionalized GQD.[4]

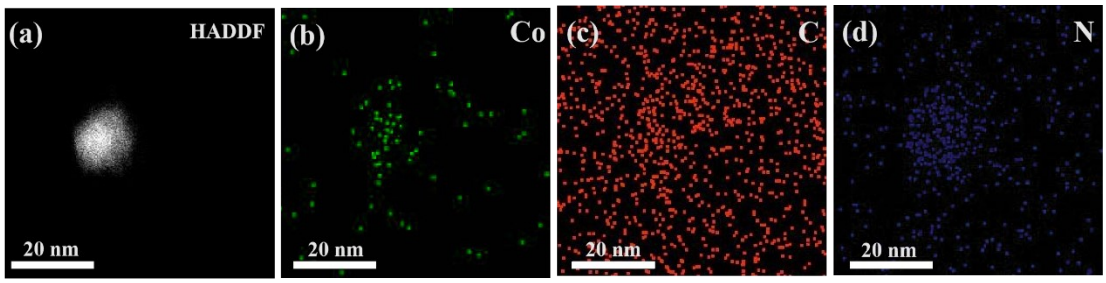

Figure S3. (a) HAADF image of CoPc/NH_2-GQD; Elemental mapping images of (b) Co, (c) C and (d) N in CoPc/NH_2-GQD.

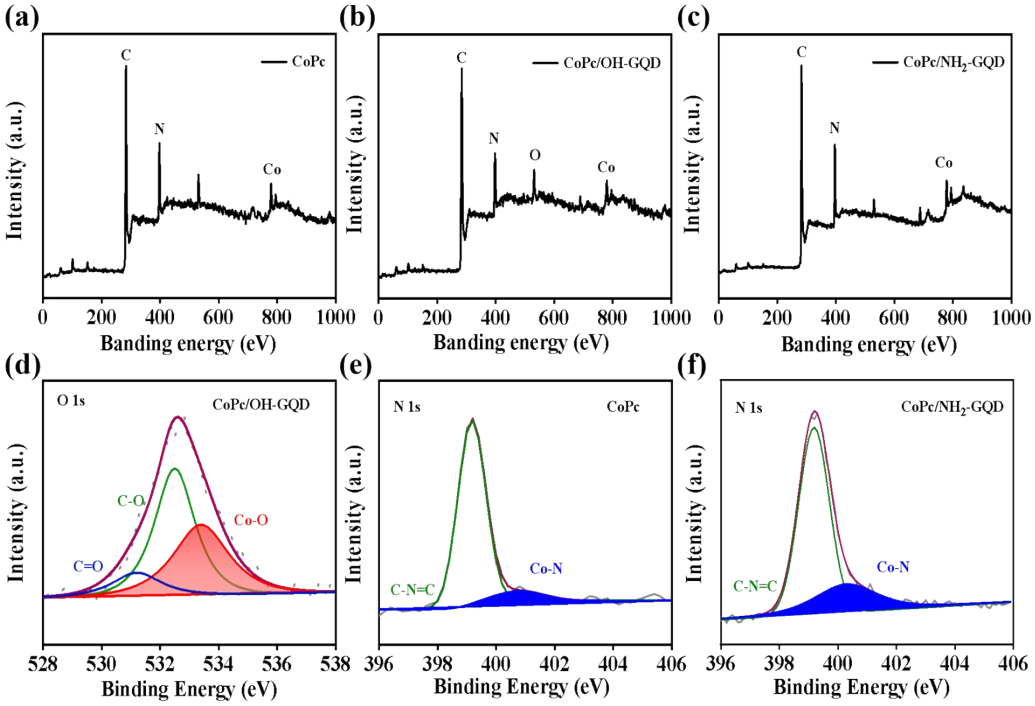

Figure S4. XPS survey of (a) CoPc, (b) CoPc/OH-GQD, and (c) CoPc/NH_2-GQD; (d) O 1s XPS spectrum of CoPc/OH-GQD; (e) N 1s XPS spectra of CoPc; (f) N 1s XPS spectra of CoPc/NH_2-GQD.

The existence of C, N, O and Co elements for CoPc/R-GQD were displayed via X-ray photoelectron spectroscopy (XPS) (Figure S4a-c). For CoPc/OH-GQD, a characteristic peak at 533.40 eV in the XPS spectra of O 1s was induced by Co-O bond, indicating the direct coordination of Co with -OH (Figure S4d).[5, 6] The N 1s high-resolution spectrum of CoPc can be deconvoluted into two main peaks at 399.1 and 400.8 eV, corresponding to C-N=C and Co-N bonds (Figure S4e).[7] The fitted ratio of the Co-N bond in CoPc/NH_2-GQD shows a significant increase when compared to CoPc (Figure S4f). This result is thus indicative for a Co-N bond in CoPc/NH_2-GQD, resulting from axial coordination of the NH_2 functionalized GQD.

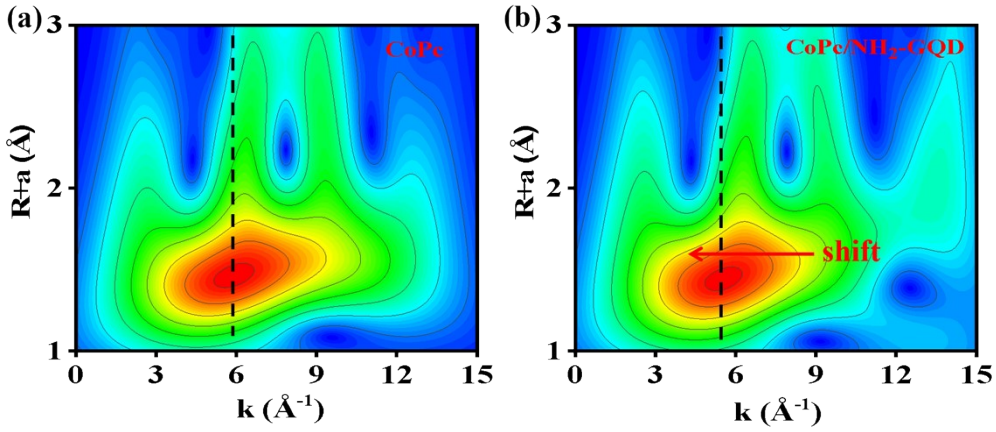

Figure S5. (a) WT analysis of CoPc; (b) WT analysis of CoPc/NH_2-GQD.

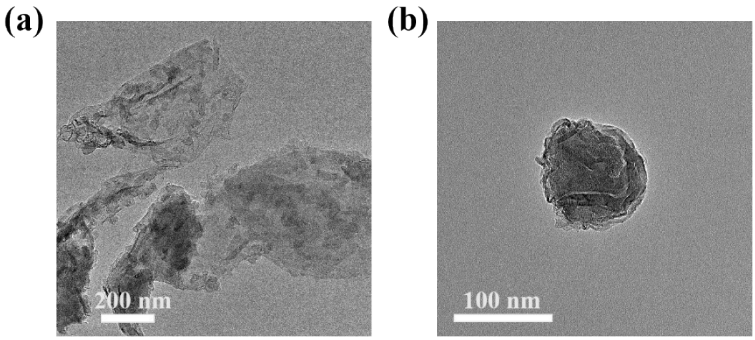

Figure S6. (a) TEM image of NH_2-G; (b) TEM image of NH_2-GNS

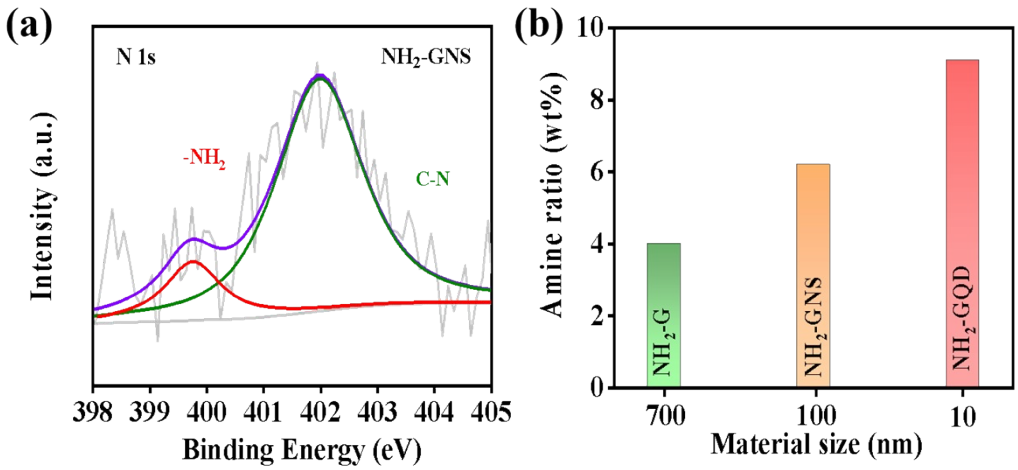

Figure S7. (a) N 1s XPS spectra of NH_2-GNS; (b) Schematic illustration of the amine ratio of materials with different sizes.

The average size of Commercial NH_2-G and NH_2-GNS is about 700 nm and 100 nm respectively (Figure S6a-b). The -NH_2 content of various materials was quantified by N 1s spectroscopy of XPS (Figure S7a) with GQD containing relatively higher -NH_2 content (Figure S7b and Table S4).

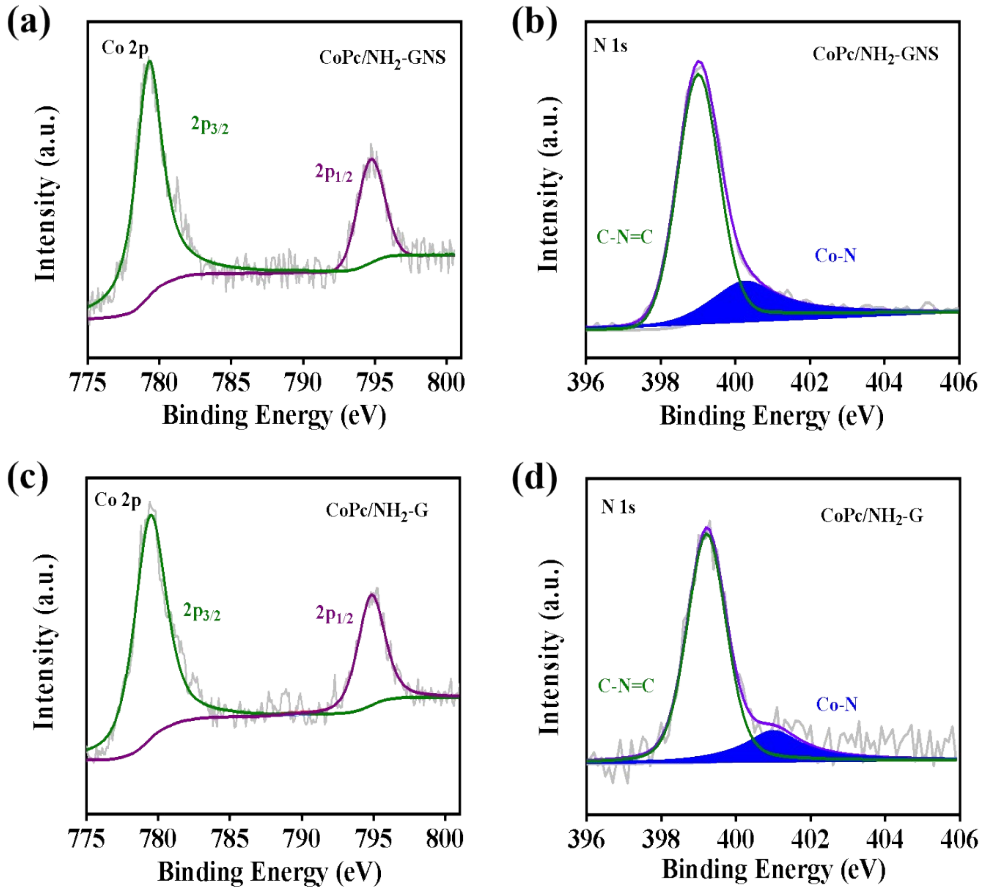

Figure S8. XPS survey of CoPc/NH_2-GNS (a) Co 2p XPS spectra; (b) N 1s XPS spectra; XPS survey of CoPc/NH_2-G (c) Co 2p XPS spectra; (d) N 1s XPS spectra.

The surface chemical composition and electronic state were investigated by XPS (Figure S8). The presence of Co-N in CoPc/NH_2-GNS and CoPc/NH_2-G were further confirmed by N 1s XPS. For Co 2p spectra, the main peaks at ~779.35 eV and ~794.90 eV in CoPc/NH_2-GNS as well as CoPc/NH_2-G are assigned to Co $2p_{3/2}$ and Co $2p_{1/2}$, with the peak of Co $2p_{3/2}$ lying between Co^0 and Co^{2+}, in agreement with the CoPc/R-GQD sample.[8] In addition, due to the electron-donating properties of -NH_2, the two main peaks (Co $2p_{3/2}$, Co $2p_{1/2}$) of CoPc/NH_2-GNS and CoPc/NH_2-G compared to pure CoPc shift ~0.31 eV and ~0.36 eV, respectively, in the direction of low binding energy (Figure S8a and c). The fitted ratio of the Co-N bond in CoPc/NH_2-GNS and CoPc/NH_2-G shows a significant increase when compared to CoPc (Figure S8b and d). This result is thus indicative for a Co-N bond in CoPc/NH_2-GNS and CoPc/NH_2-G,

resulting from axial coordination of the NH_2 functionalized graphene. In summary, CoPc is believed to be successfully assembled into NH_2-GNS and NH_2-G.

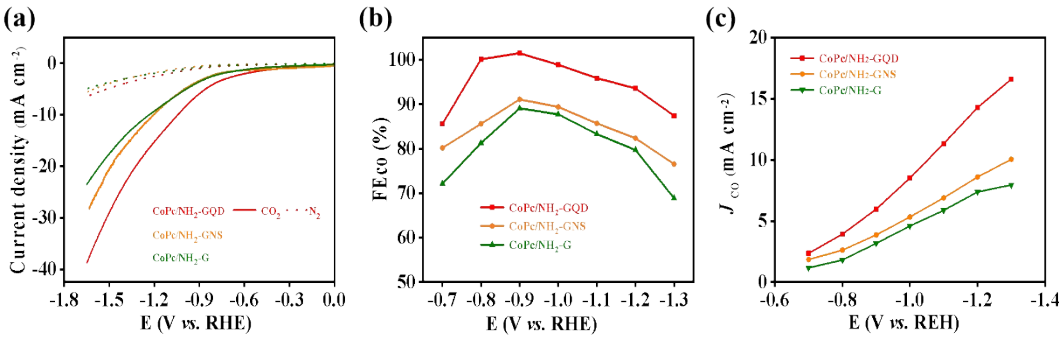

Figure S9. (a) LSV curves of CoPc/NH_2-GQD (red), CoPc/NH_2-GNS (orange), and CoPc/NH_2-G (green) in CO_2-saturated 0.1 M $KHCO_3$ solution; (b) FE of CoPc/NH_2-GQD, CoPc/NH_2-GNS, and CoPc/NH_2-G at various potentials in a typical H-cell; (c) Partial current densities of CoPc/NH_2-GQD, CoPc/NH_2-GNS, and CoPc/NH_2-G.

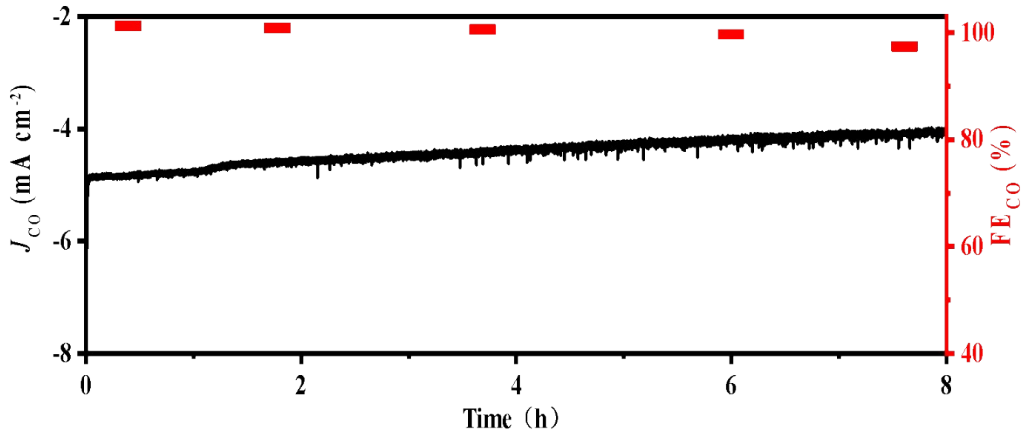

Figure S10. stability test and FE_{CO} by CoPc/NH_2-GQD at −0.8 V in CO_2-saturated 0.1 M $KHCO_3$ aqueous solution.

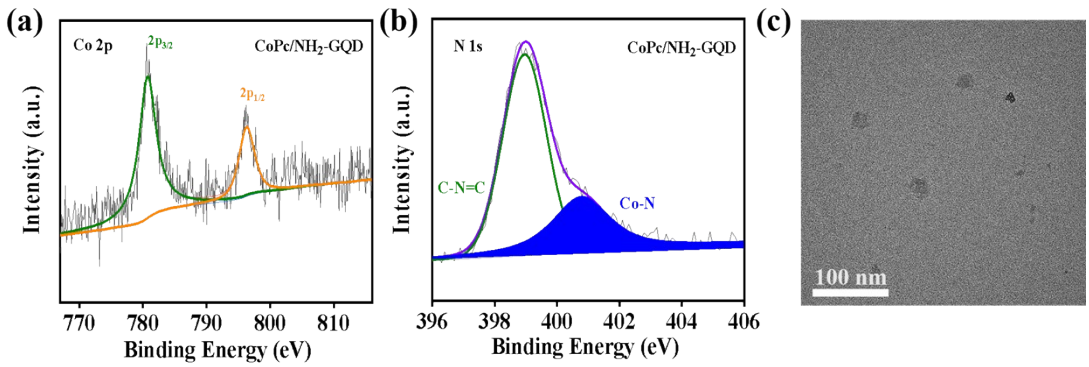

Figure S11. XPS survey of CoPc/NH_2-GQD after 8 hours of electrolysis. (a) Co 2p XPS spectra; (b) N 1s XPS spectra; (c) TEM image of CoPc/NH_2-GQD after 8 h operation at -0.8 V.

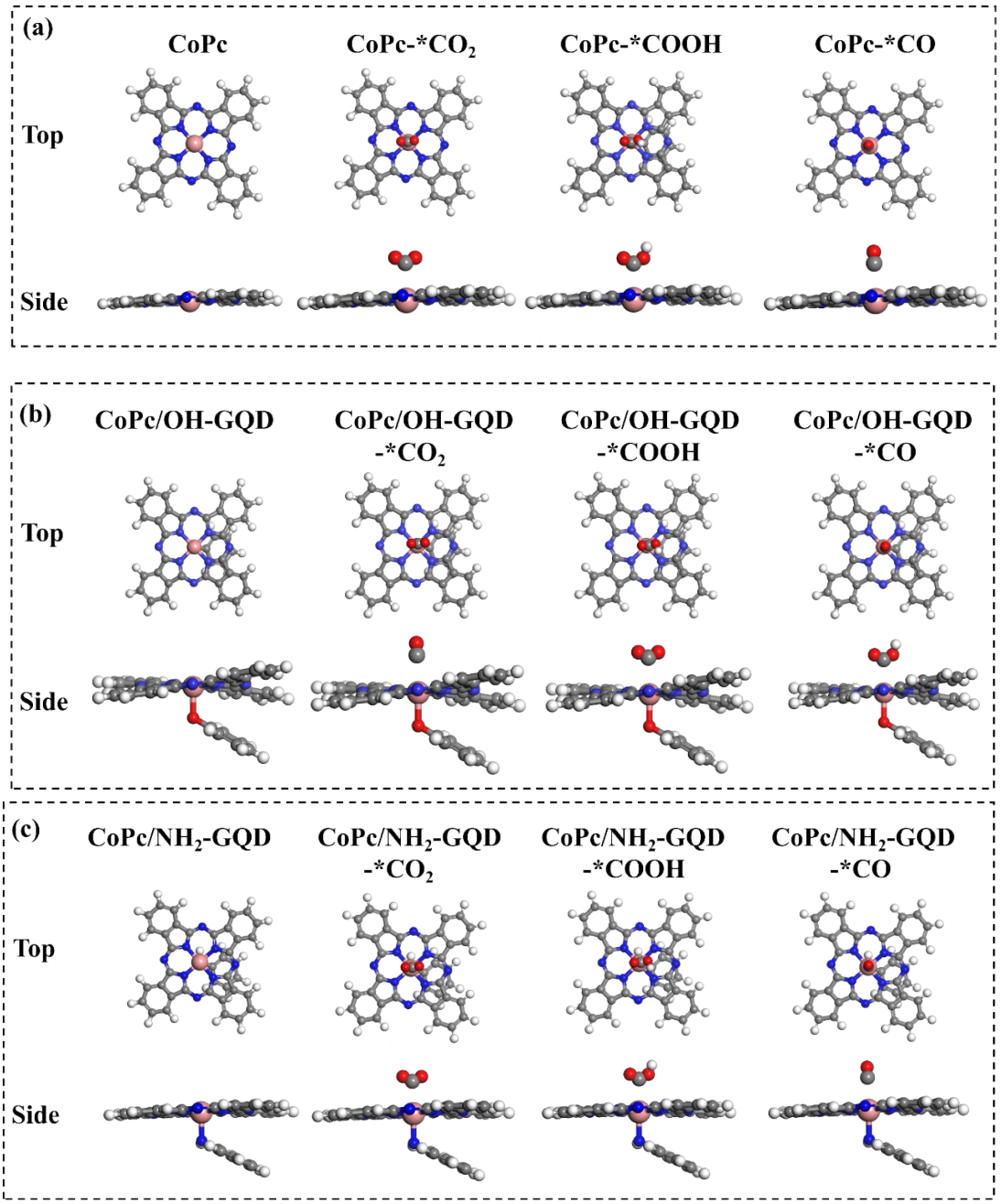

Figure S12. Structural representation of the model systems evaluated in this study: (a) CoPc, (b) CoPc/OH-GQD, and (c) CoPc/NH_2-GQD.

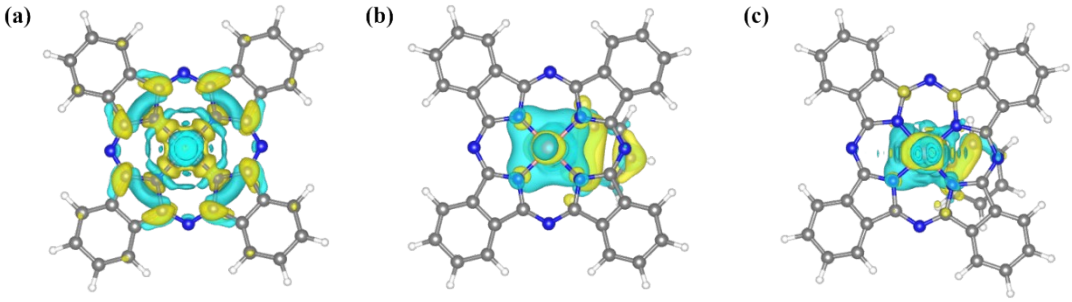

Figure S13. (a) Charge density difference of CoPc. (b) Charge density difference of CoPc/OH-GQD. (c) Charge density difference of CoPc/NH_2-GQD.

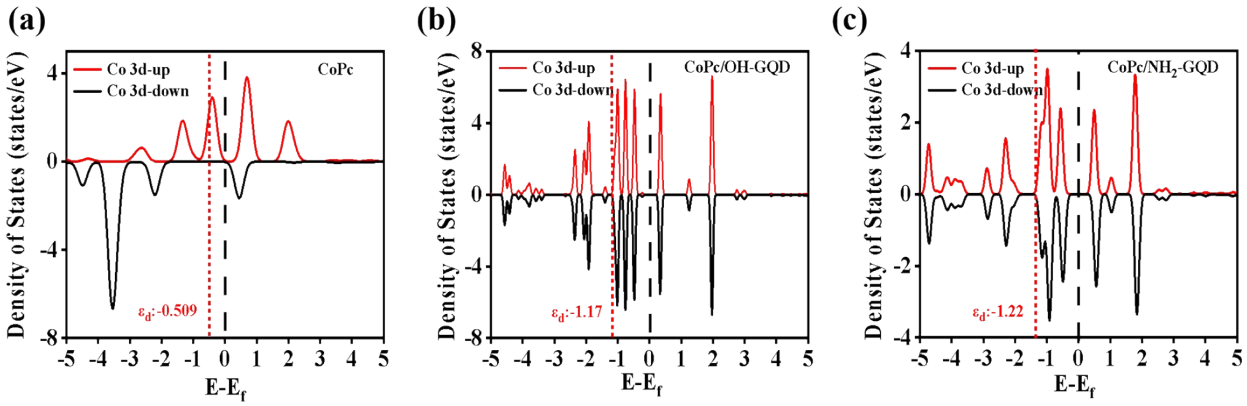

Figure S14. PDOS of (a) CoPc, (b) CoPc/OH-GQD, and (c) CoPc/NH_2-GQD.

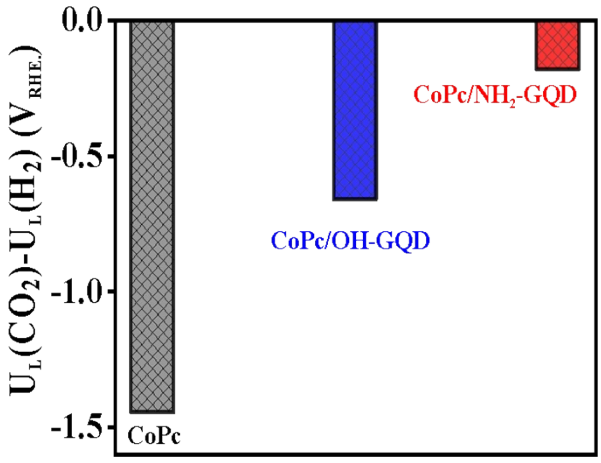

Figure S15. Limiting potential differences between CO_2 reduction and H_2 evolution on different catalyst models at U = 0 V.

Table S1. ICP-OES analysis results of the as-synthesized catalysts.

Catalyst	Co (wt.%)
CoPc/NH_2-GQD	8.35
CoPc/OH-GQD	8.27

Table S2. EXAFS fitting parameters at the Co K-edge for various samples（S_0^2=0.6973 for Co）

Sample	Shell	*CN*[a]	*R*(Å)[b]	σ^2(Å^2)[c]	ΔE_0(eV)[d]	*R* factor
Co foil	Co-Co	12*	2.49	0.006	7.7±0.2	0.0023
CoPc	Co-N	4.15	1.91	0.0012	0.46	0.018
CoPc/NH_2 -GQD	Co-N	5.2±0.3	1.86	0.003	7.5±0.6	0.0186
	Co-C	6.4±0.8	2.93	0.001		

[a]*CN*, coordination number; [b]*R*, the distance to the neighboring atom; [c]σ^2, the Mean Square Relative Displacement (MSRD); [d]ΔE_0, inner potential correction; *R* factor indicates the goodness of the fit. $S0^2$ was fixed to 0.6973, according to the experimental EXAFS fit of the sample foil by fixing CN as the known crystallographic value. This value was fixed during EXAFS fitting, based on the known structure of Co foil. Data ranges $3.0 \leq k \leq 12.0$ Å^{-1}, $1.0 \leq R \leq 3.0$ Å. The Debye-Waller factors and ΔRs are based on the guessing parameters and constrained for Co-N and Co-C.

Data reduction, data analysis, and EXAFS fitting is applied through Athena and Artemis software.[9] The energy calibration of the sample was conducted through a standard Co foil, which as a reference was simultaneously measured. For EXAFS modeling, The global amplitude EXAFS (*CN*, *R*, σ^2 and ΔE_0) were obtained by nonlinear fitting, with least-squares refinement, of the EXAFS equation to the Fourier-transformed data in R-space, using Artemis software, EXAFS of the Co foil is fitted and the obtained amplitude reduction factor S_0^2 value was set in the EXAFS analysis to determine the coordination numbers (CNs) in the scattering path in sample. The Debye-Waller factors and delta Rs are obtained based on the guessing parameters and constrained for Co-N and Co-C. Wavelet transformation (WT) is also employed using the software package developed by Funke and Chukalina using Morlet wavelet with $\kappa = 10$, $\sigma = 1$.[10, 11]

To get a better fitting result, we further considered the C around the Co atoms and adding Co-C path based on the CoPc structure. However, because of the low molecular weight of C, its impact on the signal is limited and inaccurated. Thus, the peak of Co-C path appeared to be above 2 A with a low intensity. The fitting results showed the C is surrounding with an average number of 6.

Table S3. Catalytic performance comparisons of the reported ECRR electrocatalysts with CoPc/NH_2-GQD.

Catalysts	E (V *vs.* RHE)	FE_{CO} (%)	Potential range (mV)	Electrolyte	Reference
CoPc/NH_2-GQD	**-0.8**	**~100**	**500**	**0.1 M $KHCO_3$**	**This work**
$CoPorN_3$	-0.5	96	50	0.5 M $KHCO_3$	12
COF@CoPor	-0.6	94	100	0.5 M $KHCO_3$	13
CoPc-2H_2Por	-0.55	95	100	0.5 M $KHCO_3$	14
CoPc@DNHCS-8	-0.87	95.68	300	0.5 M $NaHCO_3$	15
CoPP@CNT	-0.65	~90	100	0.5 M $NaHCO_3$	16
CoPc-py-CNT	-0.53	91	150	0.2 M $NaHCO_3$	17
Co-N/HNPCSs	-0.79	99	220	0.2 M $NaHCO_3$	18
CoPc-CNT	-0.63	92	40	0.1 M $KHCO_3$	19
CoPc/GDY/G	-0.9	96	100	0.1 M $KHCO_3$	20
Co-PPIX	-1.32	94	400	0.1 M $KHCO_3$	21
Co-C_2N_3	-0.8	92	200	0.1 M $KHCO_3$	22

Table S4. Summary of amino content in NH_2-GQD, NH_2-GNS and NH_2-G samples.

Catalyst	Amine ratio (wt.%)
NH_2-GQD	9.1
NH_2-GNS	6.2
NH_2-G	4.0

1. J. K. Nørskov, J. Rossmeisl, A. Logadottir, L. Lindqvist, J. R. Kitchin, T. Bligaard and H. Jónsson, J. Phys. Chem. B, 2004, **108**, 17886–17892.
2. R Ye, Z Peng, Andrew Metzger, J Lin, Jason A. Mann, K Huang, C Xiang, X Fan, Errol L. G. Samuel, Lawrence B. Alemany, Angel A. Martí, and James M. Tour, ACS Applied Materials & Interfaces, 2015, **7**, 7041-7048.
3. Cao H, Xing L, Wu G, Xie Y, Shi S, Zhang Y, Daisuke Minakata, John C. Crittenden, Applied Catalysis B: Environmental, 2014, 146, 169-176.
4. L. Wang, Y. Wang, T. Xu, H. Liao, C. Yao, Y. Liu, Z. Li, Z. Chen, D. Pan, L. Sun and M. Wu, *Nat. Commun*, 2014, **5**, 1–9.
5. T. Zhang, W. Li, K. Huang, H. Guo, Z. Li, Y. Fang, R. M. Yadav, V. Shanov, P. M. Ajayan, L. Wang, C. Lian and J. Wu, Nat. Commun, 2021, **12**, 1–9.
6. Y. T. Liu, X. Chen, J. Yu and B. Ding, Angew. Chemie, 2019, **58**, 18903–18907.
7. M. Li, C. Yan, R. Ramachandran, Y. Lan, H. Dai, H. Shan, X. Meng, D. Cui, F. Wang and Z. X. Xu, *Chem. Eng. J.*, 2022, **430**, 133050.
8. J. Pei, T. Wang, R. Sui, X. Zhang, D. Zhou, F. Qin, X. Zhao, Q. Liu, W. Yan, J. Dong, L. Zheng, A. Li, J. Mao, W. Zhu, W. Chen and Z. Zhuang, Energy Environ. Sci., 2021, **14**, 3019–3028.
9. B. Ravel and M. Newville, J. Synchrotron Radiat., 2005, **12**, 537-541.
10. H. Funke, A. C. Scheinost and M. Chukalina, *Phys. Rev. B*, 2005, **71**, 094110.
11. H. Funke, M. Chukalina and A. C. Scheinost, J. Synchrotron Rad., 2007, **14**, 426-432.
12. T. Wang, L. Guo, H. Pei, S. Chen, R. Li, J. Zhang and T. Peng, Small., 2021, 17, 2102957.
13. L. Zhai, S. Yang, C. Lu, C. X. Cui, Q. Xu, J. Liu, X. Yang, X. Meng, S. Lu, X. Zhuang, G. Zeng and Z. Jiang, Small, 2022, 18, 2200736.
14. J. Yuan, S. Chen, Y. Zhang, R. Li, J. Zhang and T. Peng, Adv. Mater., 2022, 34, 2203139.
15. S. Gong, W. Wang, C. Zhang, M. Zhu, R. Lu, J. Ye, H. Yang, C. Wu, J. Liu, D. Rao, S. Shao and X. Lv, Adv. Funct. Mater., 2022, 32, 2110649.

16. M. Zhu, J. Chen, L. Huang, R. Ye, J. Xu and Y. F. Han, Angew. Chem. Int. Ed., 2019, 58, 6595 – 6599.
17. M. Zhu, J. Chen, R. Guo, J. Xu, X. Fang and Y. F. Han, Appl. Catal. B Environ., 2019, 251, 112 – 118.
18. Y. Pan, R. Lin, Y. Chen, S. Liu, W. Zhu, X. Cao, W. Chen, K. Wu, W. C. Cheong, Y. Wang, L. Zheng, J. Luo, Y. Lin, Y. Liu, C. Liu, J. Li, Q. Lu, X. Chen, D. Wang, Q. Peng, C. Chen and Y. Li, J. Am. Chem. Soc., 2018, 140, 4218 – 4221.
19. X. Zhang, Z. Wu, X. Zhang, L. Li, Y. Li, H. Xu, X. Li, X. Yu, Z. Zhang, Y. Liang and H. Wang, Nat. Commun., 2017, 8, 14675.
20. Gu H, Zhong L, Shi G, Shi G, Li J, Yu K, Li J, Zhang S, Zhu C, Chen S, Yang C, Kong Y, Chen C, Li S, Zhang J, Zhang L, Journal of the American Chemical Society., 2021, 143, 8679 – 8688.
21. N.G. Yasri, T.A. Al-Attas, J. Hu, M.G. Kibria, Catal, Sci. Technol., 2021, 11, 1580 – 1589.
22. Cheng H, Fan Z, Wu X, Feng M, Zheng W, Lei G, Li X, Cui F, He G. Journal of Catalysis., 2022, 405: 634 – 640.